# FAST FACTORISED BACK PROJECTION FOR SYNTHETIC APERTURE IMAGING AND WIDE-BEAM MOTION COMPENSATION

H J Callow Norwegian Defence Research Establishment, Kjeller, Norway
R E Hansen Norwegian Defence Research Establishment, Kjeller, Norway

## 1 INTRODUCTION

Both synthetic aperture radar (SAR) and synthetic aperture sonar (SAS) require processing of the individual pulse data to generate a final image. This processing is often computationally heavy and thus both costly and time consuming. Research into reconstruction techniques has been of interest since the start of these two imaging fields and is still a popular topic today[10, 11].

Traditionally, there are two branches of reconstruction techniques in the SAR and SAS fields:

- Fourier-based algorithms, operating in the along-track Doppler or wavenumber domains have become standard for operational SAR systems and the basis for the only commercially SAS processor currently available[14]. These algorithms are fast, operate well with narrow-beam systems and are well understood.
- Time / space based algorithms, are typically used in research and can generate useful images in situations where Fourier-based algorithms can be difficult to derive and operate such as circular SAR or with extreme wide-beam systems such as CARABAS. An important disadvantage is in a significantly heavier computational burden, although this typically is not a problem in research environments.

These two separate approaches are both used in the processing chain of the Focus toolbox[2] shown in Figure 1. Due to practical considerations, full-swath imagery is expected to be passed through the left branch with Fourier beamformers and full resolution images of small regions through the time-domain reconstruction branch on the right hand side. Ideally, the two separate branches would be combined to simplify both maintenance and code optimisation; this would increase processing speed and reduce the amount of code in use.

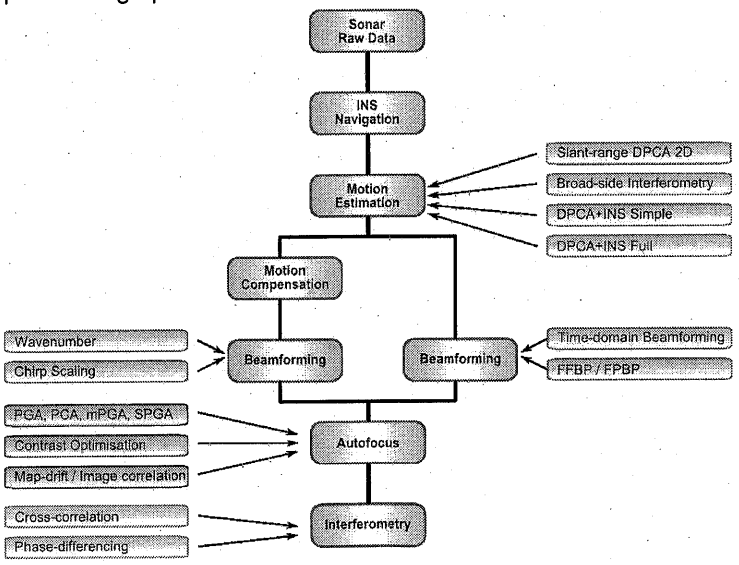


Figure 1, illustration of the two processing chains used in Focus toolbox. Typically processing choices for full swatch use the left branch and spotlight reconstruction uses the right branch.

A current topic of interest is in reconstruction where the platform carries a wide-beam sensor and also suffers significant deviation from a linear path. Fourier beamformers become more difficult to use and require more computation due to heavier motion compensation. In this scenario, Fourier beamformers require non-trivial wide-beam motion-compensation, algorithms for which have only recently been developed[9, 10].

Another set of research groups have attempted to address the situation in a parallel development. These groups are developing recursive (hierarchical) backprojection algorithms for speeding up traditional time-domain backprojection beamformers from $O(N^3)$ to $O(N^2 \log N)$.

We discuss the relative similarities and approaches used in both camps in section 3 with background on the system geometry and general notation in section 2. A novel suggestion for hybridization of FFBP and Fourier-methods is suggested in section 4.2 and a summary of the paper is presented in section 5.

# 2 SYSTEM MODEL AND NOTATION

Figure 2 below shows the typical geometry for imaging with a starboard looking sonar. The notation system used in this paper is a right-handed coordinate system that is earth-fixed; note that this requires a z-axis pointing toward the seafloor.

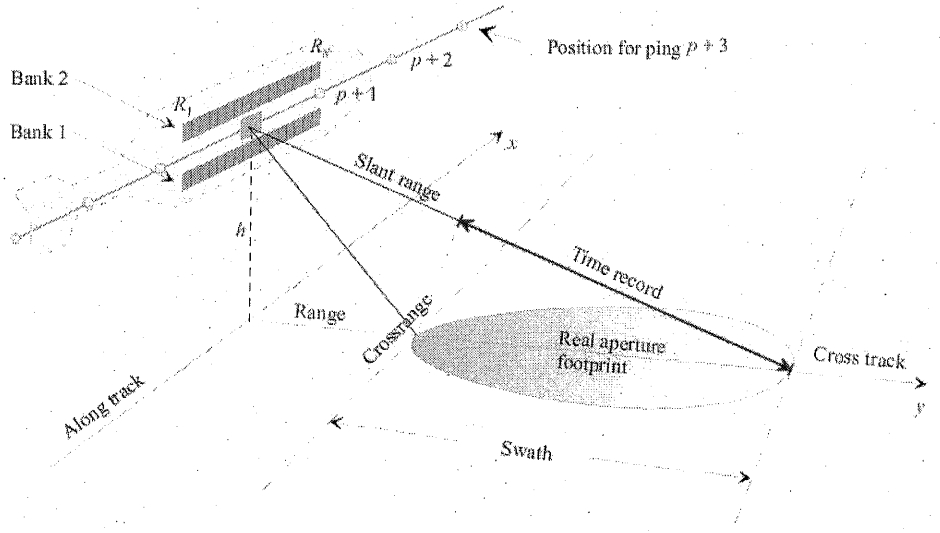


Figure 2, typical geometry for an interferometric SAS system. The echo from a given ping is recorded as a function of two-way travel time.

SAS systems typically choose a single transmitter multiple receiver / geometry to allow adequate along-track sampling for useful along-track velocities. This bistatic (multistatic really) geometry must be accounted for in the imaging processes if artefacts are to be avoided.

Writing in bistatic form and using a vector notation for position where, $\mathbf{x} \equiv (x, y, z)$, gives the recorded echo from a receiver at $\mathbf{x}_{\mathrm{rx}}$ and transmitter at $\mathbf{x}_{\mathrm{tx}}$ for a scene, $f(\mathbf{x})$:

$$s\left(k, \mathbf{x}_{\mathrm{rx}}, \mathbf{x}_{\mathrm{tx}}\right) = \iiint f\left(\mathbf{x}\right) \exp\left(-jk(||\mathbf{x}_{\mathrm{tx}} - \mathbf{x}|| + ||\mathbf{x}_{\mathrm{rx}} - \mathbf{x}||)\right) d\mathbf{x}$$

The imaging process may then be written using a matched filter in 2D as:

$$\widehat{f}\left(\mathbf{x}\right) = \iiint s\left(k, \mathbf{x}_{\mathrm{rx}}, \mathbf{x}_{\mathrm{tx}}\right) \exp\left(jk(||\mathbf{x}_{\mathrm{tx}} - \mathbf{x}|| + ||\mathbf{x}_{\mathrm{rx}} - \mathbf{x}||)\right) dk\, d\mathbf{x}_{\mathrm{rx}}\, d\mathbf{x}_{\mathrm{tx}}$$

If using a time-domain beamformer (equivalent to a backprojector) the time delay is implemented with an interpolator in time-domain instead as

$$\widehat{f}(\mathbf{x}) = \iint s\left(\tau - \tfrac{1}{c}(||\mathbf{x}_{\mathrm{tx}} - \mathbf{x}|| + ||\mathbf{x}_{\mathrm{rx}} - \mathbf{x}||), \mathbf{x}_{\mathrm{rx}}, \mathbf{x}_{\mathrm{tx}}\right) d\mathbf{x}_{\mathrm{rx}}\, d\mathbf{x}_{\mathrm{tx}}$$

The system model above has neglected range-loss terms for simplicity. In practise these terms are included in the imaging methods although may be partially compensated for through use of time varying gain (TVG) in the sonar itself.

# 3 TIME-DOMAIN RECONSTRUCTION METHODS

As noted in the introduction, there are a number of image reconstruction methods currently in use in the SAS / SAR communities. In this section we look at typical time-domain back projection, and fast factorised back projection (FFBP) an accelerated time-domain method.

## 3.1 Time-domain Back Projection

This method is regarded as the standard with which to compare other algorithms[10], this despite that the algorithms in typical use require more approximations to derive than their Fourier domain equivalents. This is due to the ease with which non-linear paths may be handled.

### 3.1.1 Beam-width limiting

An often neglected aspect in discussion of time-domain back projection for narrow-beam systems is limiting and tapering the imaging beam. This is an absolute necessity in all reconstruction methods and has been discussed in relation to aperture undersampling, for example in Gough and Hawkins[3].

The Doppler limiting discussed in Gough and Hawkins[3] can also be applied in straightforward fashion to time-domain backprojectors using a narrow-band approximation where $k_x = 2k_0 \sin\theta$. Thus the imaging and sampling limits of D/3=0.66 * 0.88 $\theta_{3dB}$ used in SAS reconstruction can be included in the backprojection by limiting $\theta$. As an extension of the technique, standard Hamming weighting should be applied as a function of $\theta$ to obtain useful impulse responses.

Often in spot reconstruction of small regions, this tapering is instead applied as a function of array position instead of angle. Another implicit technique often used is to apply the backprojection only over the pings that see the target region. Neither of these angular limiting techniques will work well on large scenes or with FFBP.

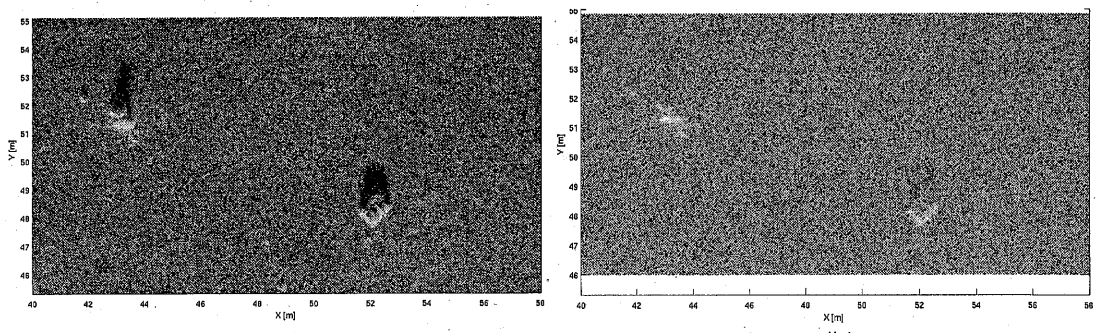


(a) (b)

Figure 3, effect of beam limiting. Image (a) shows a time-domain reconstructed image with explicit beam tapering as a function of angle. Image (b) is the same scene without tapering applied. Aperture length is 2-3 times longer than necessary to reconstruct (b) and thus undersampling occurs.

The effect of neglecting this limiting may clearly be seen in Figure 3 which is a small region taken from a large scene. Image (a) has had the tapering applied and image (b) has not. It is also worth

noting that the processing time drops significantly if tapering is in use; from 484 seconds to 191 seconds.

This angular limiting has an enormous effect on discussions regarding computational burden as the angular limit also limits the N over which the order of computation calculations are derived from. In a narrow-beam system N can be very small (of order 100) and standard assumptions about processing costs are no longer valid. This is particularly important for extremely narrow-beam systems where time-domain back projectors may be relatively inexpensive. For the images above, N is a relatively small 114 because of the short imaging range of around 50m even though a wide-beam sonar has been used.

## 3.2 Fast Factorised Back Projection (FFBP[6])

FFBP and similar methods rely on a recursive partitioning of the back projection integral to allow what in effect amounts to a far-field approximation at each recursive stage[6, 7]. This approximation greatly reduces the computational burden faced in the back-projection by allowing localised regions in the image to be calculated with a single square root. By varying the amount of approximation, the processing cost may be varied between that of the standard backprojector and a Fourier beamformer[7].

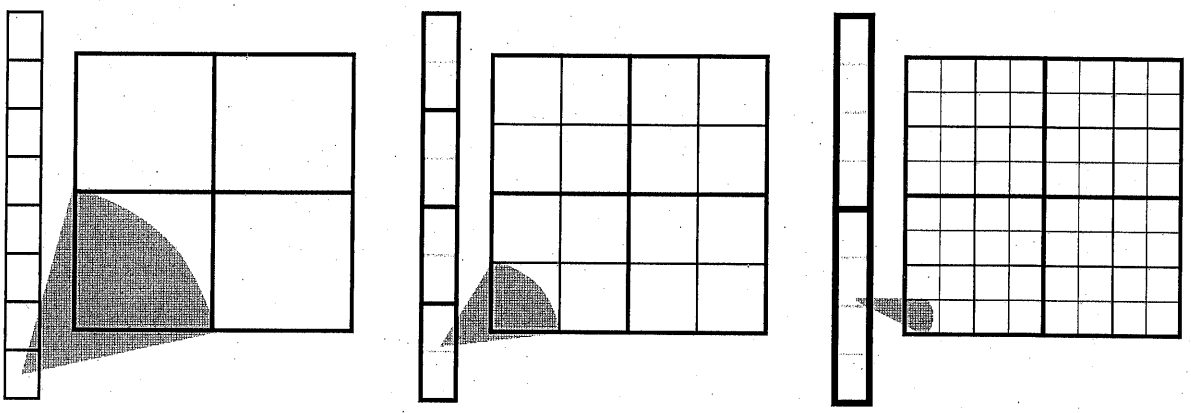

Figure 4. Recursive nature of FFBP, stage 0 to stage 3 left to right. All values in a square at a given stage are approximated with a single square root term. Elements are combined in a given direction to reduce beam angle and thus the approximation error. Approximation beamwidth (grey) is typically 3-5 times narrower than full system beamwidth dependent on the chosen level of approximation.

### 3.2.1 Approximation error

The processing speed of FFBP is closely controlled by an approximation factor Efact. For a given number of recursive factorisation stages this factor alone determines the processing speed gain over a traditional backprojector. With no approximation error, FFBP will have the same or worse processing cost as a traditional backprojector[8]. This approximation is therefore extremely important.

We see from Ulander et al[6] that the approximation comes about from assuming all reflectors in a given sub patch lie along the centre line of the patch. Reflectors away from the centre line, end up with a phase error proportional to distance from the centre line. Interestingly, this phase error is almost linear with increasing distance and thus encodes angular position relative to the centre line.

Starting with the terms from Ulander[6] the approximation error for an aperture length, $L_A$ and image along-track size $L_I$ is given by

$$|\Delta r_{\max}| = \frac{L_A L_I}{4 r_{\min}}$$

This gives the normalised error Efact[7] in the notation of this paper as

$$E_{\text{fact}} = \frac{L_A L_I}{4\lambda \, ||\mathbf{x} - \mathbf{x}_{\text{rx}}||_{\min}}$$

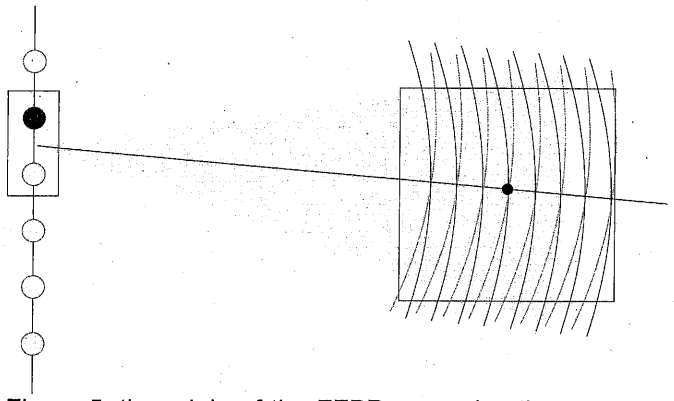

Figure 5, the origin of the FFBP approximation error is in treating all scatterers in a patch as if they were at the centre of the patch.

Approximation error in FFBP is a particularly interesting topic given that it is the main driver for the algorithm's speed improvement. A number of attempts to reduce the error through angular interpolation have been made[7, 11, 12]; these attempts will reduce error and allow faster processing. Interestingly the "approximation error" itself contains useful information about target location that may be possible to exploit inside the beamforming (as the Fourier beamformers do).

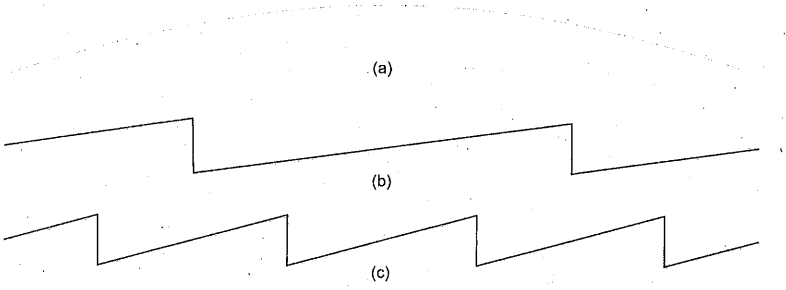


Figure 6, FFBP approximation error as a function of image location at varying stages. (a) Aperture phase function and beam limiting. (b) Recursive stage 1. (c) Recursive stage 2. Note maximum error is the same for both stages.

Note that the approximation error appears as a sawtooth phase function. The effect of this is to cause multiple repetitions of the Doppler spectrum and thus ambiguous, smeared targets in the final image. The location of the ambiguous target energy in the image is possible to calculate from the period of the sawtooth and its odd harmonic locations. For each stage, different ambiguous energy locations exist, some cancelling with energy from other stages.

### 3.2.2 Beam-width limiting

Beam limiting with respect to FFBP has yet to be discussed in great detail in the literature. The technique has been implemented in this paper, in Ødegaard[8], and at least mentioned by the authors of 11 with regard to standard back-projection. We expect that this aspect of time-domain backprojection will be discussed in more detail as FFBP and the like are used more frequently.
In our implementation the beam-width limiting used for a standard time-domain beamformer is applied in all recursive stages and the tapering is applied only in the last stage (the backprojection). Although this leads to lower resolution on the tapering and limiting accuracy for a small number of stages the approximation seems to be valid. In addition, because the angular limiting prevents

signal energy aliasing in the recursive stages, the effect of the FFBP approximation error Efact[7] becomes more predictable.

### 3.2.3 Similar methods

FFBP has a number of closely related algorithms that are not discussed in this paper[6, 7]. Note however that beam-width limiting may already be inherent in some of these; for example in Fast Polar Back Projection (FPBP)[7, 12].

### 3.2.4 Experimental results

To test the FFBP implementation, a synthetic scene was created with a full bistatic sonar simulator. In order to make the results more applicable to those from the field collected data shown later a HiSAS 1030 system[16] was modelled with a number of isolated point scatterers at various ranges.

Various reconstructions were performed with a bistatic FFBP implementation at the nominal range of 56 metres and both the number of FFBP stages and the amount of approximation were varied. Care must be taken in interpreting the various Efacts shown in this section as they are derived for a monostatic system. With a bistatic FFBP only the receiver path-length is approximated at the recursive stages effectively halving the approximation error[15].

The aim of the testing was to find the FFBP approximation level giving reasonable reconstruction performance. We have therefore reconstructed the same image scene with a standard time-domain beamformer and FFBP with varying approximation level and total stages. Beam tapering was applied as discussed earlier in the paper.

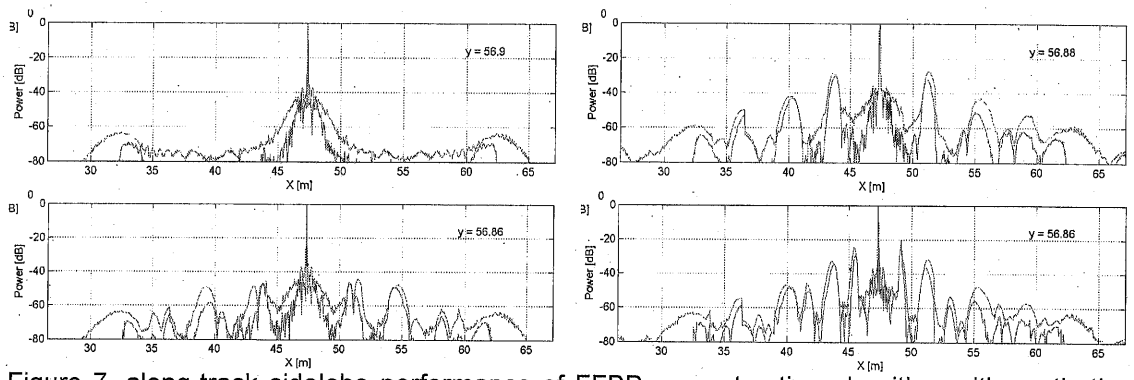


Figure 7, along-track sidelobe performance of FFBP reconstruction algorithm with synthetic data. Clockwise from top left: traditional backprojection (no approximation); FFBP with 2 stages and Efact = 1/5; FFBP with 3 stages and Efact = 1/5; FFBP with 2 stages and Efact = 1/10. Red line: sidelobes corresponding to target range; magenta line: maximum sidelobe level.

The results, summarised in Figure 7, indicate that alias location and energy is a function of the total number of stages as well as approximation error. FFBP with 3 recursive stages shows alias energy at twice as many locations and generally higher alias lobes for a given Efact. In addition, the aliasing predicted from a sawtooth approximation error is evident in the location and smearing of the approximation-induced alias energy.

In a second test, mimicking the first, the same FFBP parameter sets were used on field-collected data obtained from the SENSOTEK system[1]. In order to compare results with a hypothetical HiSAS 1030 system, receiver array elements have been coupled 2 and 2 to reduce the beamwidth and resolution of the system. Motion-estimation has been performed using DPCA[13] and sound speed estimated through autofocus techniques[17].

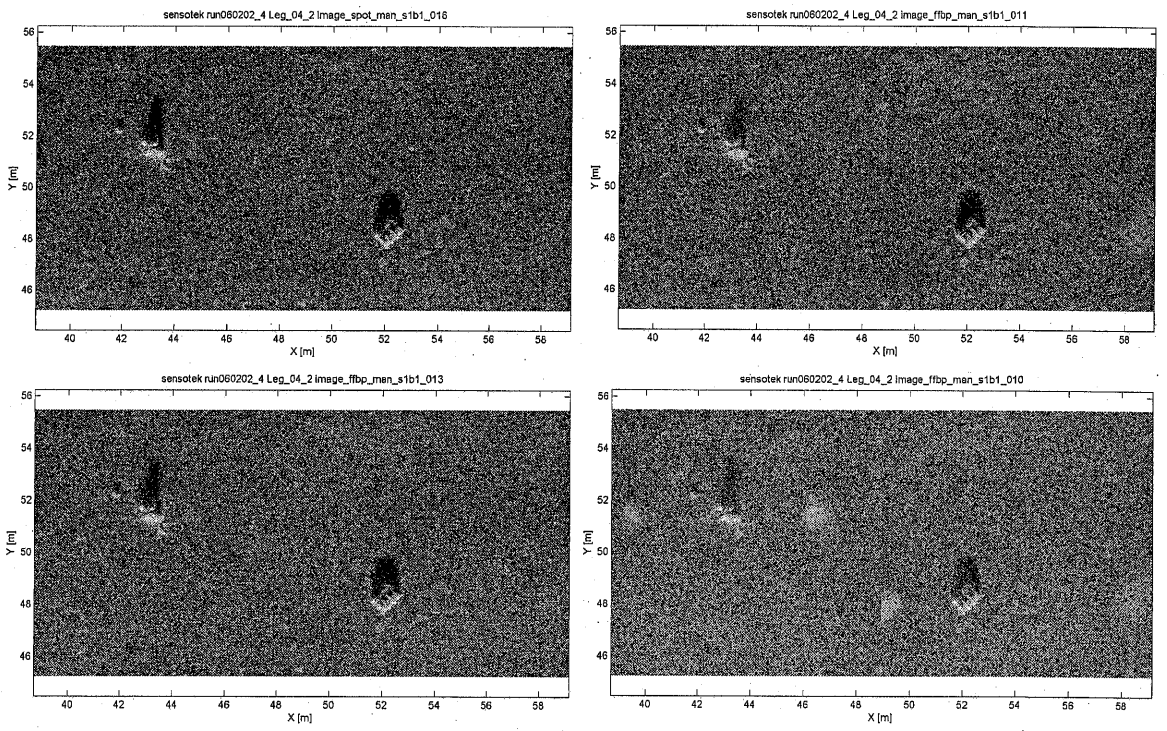


Figure 8, imaging performance of FFBP reconstruction algorithm field data. Clockwise from top left: traditional backprojection (no approximation); FFBP with 2 stages and Efact = 1/5; FFBP with 3 stages and Efact = 1/5; FFBP with 2 stages and Efact = 1/10.

From the images shown in Figure 8 summarising the results it is possible to discern the same trends noted with synthetic data. Larger approximations result in higher levels of ambiguous energy that is smeared out over the image. It is also possible to notice some degradation in the bottom left image when compared with the benchmark backprojection image. From these results it is possible to conclude that Efact must be better than 1/10 for reasonable imaging with this sonar and geometry.

Reconstruction times for FFBP are generally faster than for the traditional time-domain back projection although not startlingly so. On the image sets above, the reconstruction time for FFBP is between 20%—80% of the traditional backprojector depending on Efact and the number of stages. This is roughly in line with that seen in other SAS FFBP implementations[7]. Not much better than this can be expected for a scene with such low N. Given N=114 independent pings-on-target the theoretical best order of computation gain is N / log2(N) = 15 for Efact = ½ and about 5 for Efact = 1/10. The additional complexity of FFBP makes achieving the theoretical performance improvement difficult.

# 4 DOPPLER/WAVENUMBER DOMAIN METHODS

Reconstruction methods exploiting the Doppler or wavenumber domains have become standard in airborne SAR reconstruction[13]. Although fast, Fourier methods are cannot natively compensate for non-straight flight geometries requiring pre-processing or motion-compensation to account for non-straight geometry and bistatic collection. The motion-compensation determines the accuracy with which images from non-linear flight paths may be processed.

We demonstrate that motion-compensation may be written as a back projection followed by a forward projection. This leads to a potential hybrid using FFBP for motion compensation and the wavenumber algorithm for imaging.

As the wavenumber, Chirp-scaling, and range-Doppler algorithms are well covered elsewhere[3,4,13] we will not discuss their implementation further in this paper.

### 4.1.1 Motion compensation

Motion compensation refers to coercing the recorded echo data into the form of that from a monostatic, linear-track equivalent system. Earlier this comprised of a simple time-delay to the data but as systems have become more wide-beam more effort is required.

Full motion compensation may be looked at as projecting the data onto a new trajectory (one which fulfils the linear-track constraint). This projection can be modelled as simulating data given an image estimate. Using the system model from section 2 above allows us to write the motion compensated echo data as

$$s\left(k, \mathbf{x}_{\mathrm{pca}}\right) = \iiint \widehat{f}\left(\mathbf{x}\right) \exp\left(-j2k \left|\left|\mathbf{x}_{\mathrm{pca}} - \mathbf{x}\right|\right|\right) d\mathbf{x}$$

Where $\mathbf{x}_{\mathrm{pca}}$ is the location of the equivalent straight-line monostatic receiver and $\hat{f}(\mathbf{x})$ is an estimate of the scene over the region of interest. Substituting the original time-domain backprojected image estimate or $\hat{f}(\mathbf{x})$ allows us to write the motion-compensated data as a function of the original bistatic echo data as

$$s\left(k, \mathbf{x}_{\mathrm{pca}}\right) = \iiint \left( \iiint s\left(k, \mathbf{x}_{\mathrm{rx}}, \mathbf{x}_{\mathrm{tx}}\right) \exp\left(jk'\left(\left|\left|\mathbf{x}_{\mathrm{tx}} - \mathbf{x}\right|\right| + \left|\left|\mathbf{x}_{\mathrm{rx}} - \mathbf{x}\right|\right|\right)\right) dk' \, d\mathbf{x}_{\mathrm{rx}} \, d\mathbf{x}_{\mathrm{tx}} \right) \exp\left(-j2k \left|\left|\mathbf{x}_{\mathrm{pca}} - \mathbf{x}\right|\right|\right) d\mathbf{x}$$

simplifying and writing instead as a time-domain interpolation we get

$$s\left(\tau, \mathbf{x}_{\mathrm{pca}}\right) = \iiint \iint s\left(\tau - \tfrac{1}{c}\left(\left|\left|\mathbf{x}_{\mathrm{tx}} - \mathbf{x}\right|\right| + \left|\left|\mathbf{x}_{\mathrm{rx}} - \mathbf{x}\right|\right| - 2\left|\left|\mathbf{x}_{\mathrm{pca}} - \mathbf{x}\right|\right|\right), \mathbf{x}_{\mathrm{rx}}, \mathbf{x}_{\mathrm{tx}}\right) d\mathbf{x}_{\mathrm{rx}} \, d\mathbf{x}_{\mathrm{tx}} \, d\mathbf{x}$$

The equation above implies taking echo data, running image reconstruction using a time-domain beamformer and then simulating data at the desired locations. The integral over 5 dimensions implies a heavy computational cost.

In practise the burden is not particularly heavy as the 3D integral over space, **x,** has its extent limited by data support, typically it is implemented as an integral over slant-range $r = c\tau/2$ and angle $\theta$. For a narrow-beam system $\theta \approx 0$ and as illustrated in Figure 9 the error in that case is small.

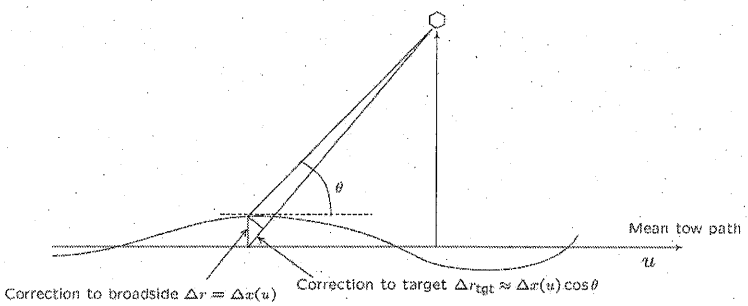


Figure 9, motion compensation with wide-beam systems requires angular dependent correction[13].

A number of different ways of implementing the motion compensation equation above exist. Beamforming for each ping into *(r, θ)* motion-compensating and then converting back to echo data, and also short-term FFTs and 2D filters are two methods used to attack the problem.

## 4.2 Hybrid method

The motion compensation method shown above is a projection from a non-linear grid to a linear one; FFBP can thus be used to complete the projections allowing a different choice in approximations for motion compensation.
Why this is desirable is evident from the FFBP approximation error noted above; the approximations from forward and backward FFBP usage cancel out. This makes the approximation error

proportional to the motion-compensation range instead of range itself. Thus for a linear-path, FFBP used for motion-compensation has no approximation at all. Even better, as long as the distance from the real path to the linear path is smaller than the range to target the approximation error is always smaller than the Efact given above. In this scenario Efact is now given by

$$\begin{aligned} E_{\text{fact mocomp}} &= \frac{L_A L_I}{4\lambda\,||\mathbf{x}-0.5\,(\mathbf{x}_{\text{rx}}+\mathbf{x}_{\text{tx}})||} - \frac{L_A L_I}{4\lambda\,||\mathbf{x}-\mathbf{x}_{\text{xp}}\,||} \\ &\approx E_{\text{fact}} \frac{||\mathbf{x}-0.5\,(\mathbf{x}_{\text{rx}}+\mathbf{x}_{\text{tx}})|| - ||\mathbf{x}-\mathbf{x}_{\text{xp}}||}{||\mathbf{x}-0.5\,(\mathbf{x}_{\text{rx}}+\mathbf{x}_{\text{tx}})|| + ||\mathbf{x}-\mathbf{x}_{\text{xp}}||} \end{aligned}$$

which for typical geometries is between 10 and 100 times smaller than Efact. As the approximation error guides the reconstruction cost, fewer FFBP recursive stages are needed and the image size at a given stage may be increased to speed up motion compensation.

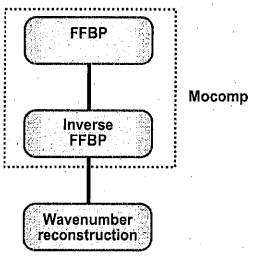


Figure 10, use of FFBP for motion compensation. Approximation errors cancel in the forward and inverse FFBP leading to the possibility of faster beamforming.

In order to test the hybrid method, a modified FFBP was made. This method does not call the traditional back-projector at the end of the recursive stages but instead recursively generates echo data from the FFBP sub-products (an inverse FFBP). Instead of calling a Fourier beamformer a traditional time-domain beamformer was used in the final image focusing due to the bistatic nature of the current FFBP implementation.

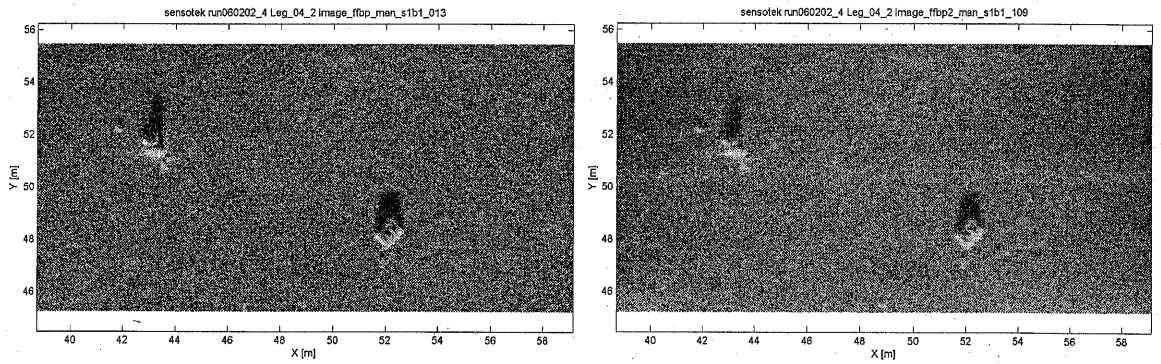


Figure 11, comparison of prototype hybrid implementation with traditional backprojector. (a) Traditional backprojector. (b) Hybrid using forward and backward FFBP for motion compensation along with traditional backprojector for final imaging. Motion-compensation used 2 recursive stages of FFBP and an Efact of 1/3. Some image degradation is visible particularly along the subpatch boundaries where echo data amplitudes were not properly normalised in the inverse FFBP algorithm. Note that the image is much better than normal FFBP for equivalent Efact indicating forward and backward approximations in the motion compensation cancel out.

# 5 CONCLUSIONS

Time-domain and Doppler/wavenumber domain imaging algorithms should not be treated as two separate subjects; methods in both domains provide insight into fast beamforming that can be beneficial. Importantly, motion compensation, as used in Fourier-based methods to allow non-linear

geometries, may be modelled as a projection. This allows use of FFBP for motion-compensation only—a simple and cheap operation compared with full reconstruction using FFBP.

Hybridising FFBP and Fourier methods in this way offers arbitrary geometry and low memory consumption as well as the high speed of fixed-geometry Fourier-based methods. In addition, the number of recursive stages in the FFBP-based motion compensation is a function of deviation from straight-line; with little or no deviation, the method collapses to traditional narrow-beam motion compensation.

### 5.1 Future work

There is scope for further work in removing or improving on the FFBP approximation error. This error essentially governs the speed of reconstruction / motion compensation. Improvements such as better azimuth interpolation used in FPBP, which reduce the approximation error through higher-order interpolation, have not yet been investigated. Better understanding of the approximation may also lead to the possibility of approximation-free FFBP for linear-geometry imaging.

## 6 REFERENCES


1. P. E. Hagen, R. E. Hansen, K. Gade, and E. Hammerstad, "Interferometric synthetic aperture sonar for AUV based mine hunting: The SENSOTEK project," in Proceedings of Unmanned Systems 2001, Baltimore, MD, USA, July-August 2001.
2. R. E. Hansen, T. O. Sæbø, H. J. Callow, P. E. Hagen, and E. Hammerstad, "Synthetic aperture sonar processing for the HUGIN AUV," in Proceedings of Oceans '05 Europe, Brest, France, June 2005.
3. P. T. Gough, and D. W. Hawkins, "Imaging algorithms for strip-map synthetic aperture sonar: minimising the effects of aperture errors and aperture undersampling", IEEE Ocean. Eng. 1997, vol 22(1), pp 27-39
4. M. Soumekh, Synthetic Aperture Radar Signal Processing. Wiley-Interscience, 1999.
5. H. J. Callow, "Signal processing for synthetic aperture sonar image enhancement", Ph.D. dissertation, University of Canterbury, Christchurch, New Zealand, April 2003.
6. L.M.H Ulander, H. Hellsten, and G. Stenstrom, "Synthetic aperture radar processing using fast factorized back-projection", IEEE Aerosp. Electron. Syst., 2003 vol 39(3), pp. 760-776
7. G. Shippey, S. Banks, J. Pihl, "SAS image reconstruction using fast polar backprojection: comparisons with fast factored back projection and Fourier-domain imaging" in Proceedings of Oceans '05 Europe, Brest, France, June 2005
8. N. Ødegaard, "Fast time domain beamforming for synthetic aperture sonar", Masters. dissertation, University of Oslo, Oslo, Norway, December 2004
9. A. S. Milman , "The hyperbolic geometry of SAR imaging", Unpublished work
10. A. Reigber, E. Alivizatos, A. Potsis, A. Moreira, "Extended wavenumber-domain synthetic aperture radar focusing with integrated motion compensation", IEE Proc.-Radar Sonar Navig. 2006, vol 153(3), pp. 301-310
11. P. O. Frölind and L.M.H. Ulander, "Evaluation of angular interpolation kernel in fast back-projection SAR processing", IEE Proc. Radar Sonar Navig. 2006, vol 153(3), pp. 243-249
12. A Olofsson. "Signalbehandling i flygburen ultrabredbandig lågfrekven-SAR i realtid", Masters dissertation, Chalmers University, July 2004 (in Swedish)
13. H. Callow, T. O. Sæbø, R. E. Hansen, "Towards robust quality assessment of SAS imagery using the DPCA algorithm" in Proceedings of Oceans '05 Europe, Brest, France, June 2005
14. ProSAS SAS processor homepage, http://www.appsig.com/business_areas/sas.htm
15. Y. Ding, and D. C. Munson, Jnr, "A fast back-projection algorithm for bistatic SAR imaging", in Proceedings of Inter. Conference on Image Proc. 2002, pp 449-452
16. P. E. Hagen, R E Hansen, B. Langli, "Synthetic Aperture Sonar for the HUGIN 1000-MR AUV", in Proceedings of UDT Europe 2006.